PLOS ONE

RESEARCH ARTICLE

Quantum simulation of particle creation in curved space-time

Raphael P. Schmit[1]*, **Bruno G. Taketani**[1,2], **Frank K. Wilhelm**[1]

1 Theoretical Physics, Saarland University, Saarbrücken, Germany, **2** Departamento de Física, Universidade Federal de Santa Catarina, Florianópolis, SC, Brazil

* raphael.schmit@lusi.uni-sb.de

Citation: Schmit RP, Taketani BG, Wilhelm FK (2020) Quantum simulation of particle creation in curved space-time. PLoS ONE 15(3): e0229382. https://doi.org/10.1371/journal.pone.0229382

Editor: Francesco Piazza, Max-Planck-Institut fur Physik komplexer Systeme, GERMANY

Received: June 8, 2018

Accepted: January 9, 2020

Published: March 6, 2020

Data Availability Statement: All relevant data are within the paper and its Supporting Information files.

Funding: This work was partially supported by the European Union through the project ScaleQIT - "Scalable Superconducting Processors for Entangled Quantum Information Technology" (https://www.chalmers.se/en/projects/Pages/Scalable-Superconducting-Processors-for-Entangled-Quantum.aspx). Bruno G. Taketani also acknowledges support from Fapesc - "Fundação de Amparo à Pesquisa e Inovação do Estado de Santa Catarina" (http://www.fapesc.sc.gov.br/) and CNPq

Abstract

Conversion of vacuum fluctuations into real particles was first predicted by L. Parker considering an expanding universe, followed in S. Hawking's work on black hole radiation. Since their experimental observation is challenging, analogue systems have gained attention in the verification of this concept. Here we propose an experimental set-up consisting of two adjacent piezoelectric semiconducting layers, one of them carrying dynamic quantum dots (DQDs), and the other being p-doped with an attached gate on top, which introduces a space-dependent layer conductivity. The propagation of surface acoustic waves (SAWs) on the latter layer is governed by a wave equation with an effective metric. In the frame of the DQDs, this space- and time-dependent metric possesses a sonic horizon for SAWs and resembles that of a two dimensional non-rotating and uncharged black hole to some extent. The non-thermal steady state of the DQD spin indicates particle creation in form of piezophonons.

1 Introduction

The ubiquitous presence of vacuum fluctuations is arguably one of the most surprising effects of quantum theory. Their existence is indirectly observable via the modification of the electron's magnetic moment [1] or the Lamb shift of an atomic spectrum [2]. A more direct access could be accomplished by converting the virtual particles into directly observable real ones. Such particle creation is predicted to take place under various conditions such as the dynamical Casimir effect [3, 4] and related circumstances [5], during the expansion of the universe [6], or due to the presence of a black hole's event horizon [7]. While the dynamical Casimir effect has been experimentally verified [8], direct experimental investigations for the two latter theoretical predictions are more challenging. Black hole analogues were first considered by W. Unruh [9] as a means to overcome this difficulty. He discovered that the propagation of sound waves in an irrotational fluid is governed by an effective metric matching that of a gravitating spherical, non-rotating massive body in Painlevé-Gullstrand coordinates [10] with line element

$$ds^2 = -[c_s^2 - v^2(r)]dt^2 + 2v(r)drdt + dr^2 + r^2 d\Omega^2 \quad (1)$$

INCT-IQ (465469/2014-0) - "Conselho Nacional de Desenvolvimento Científico e Tecnológico" (http://cnpq.br/). We acknowledge support by the Deutsche Forschungsgemeinschaft (DFG, German Research Foundation) and Saarland University within the funding programme Open Access Publishing. The funders had no role in study design, data collection and analysis, decision to publish, or preparation of the manuscript.

Competing interests: The authors have declared that no competing interests exist.

with the speed of sound c_s and flow speed $v(r)$ of the fluid. Similarly, physical systems [11–15] giving rise to an effective metric matching the Friedmann-Lemaître-Robertson-Walker line element

$$ds^2 = -c^2dt^2 + a^2(t)d\mathbf{r}^2 \tag{2}$$

can mimic a universe that expands according to the scale factor $a(t)$.

A vast number of analogue systems have been investigated, such as black hole analogues in liquid Helium [16], dc-SQUID transmission lines [17], electromagnetic wave-guides [18], water waves [19–21], hydrodynamic microcavity polariton flow [22], optical set-ups [23, 24, 24–26] and Bose-Einstein condensates [27, 28]. Systems analogue to particle creation in the dynamical Casimir effect [29, 30] and in an expanding universe [13, 14, 31] have also been proposed in systems ranging from trapped ions and BEC to photonic crystal fibers.

In this paper, we present an experimental set-up (see Fig 1) with features resembling both analogues of a black hole [16–20, 22–27] and of an expanding universe [11–15] and discuss particle creation in this system. We investigate the 1-dimensional propagation of surface acoustic waves (SAWs) on a piezoelectric p-type semiconducting substrate with an inhomogeneous 2-dimensional electron gas (2DEG) [32–34]. These systems have been widely used, e.g. to probe quantum effects in 2DEGs [35], as well as for electron transport [36, 37]. SAWs have also been proposed as a quantum computation platform [38] and for quantum simulations [39]. An attached gate allows for a controlled spatial modulation of the 2DEG density [40]. Similar to Unruh's proposal [9], this introduces a space-dependent modulation of the SAW speed. For an observer moving along the SAWs the substrate corresponds to a flowing medium carrying excitations. In the rest frame of the moving observer the SAW propagation will be described by an effective metric giving rise to a sonic horizon for SAWs at the crossover between subsonic and supersonic propagation. This indicates particle creation in form of piezoelectric phonons. A possible implementation of a moving particle detector using dynamic quantum dots (DQDs) is also discussed.

This paper is organized as follows. In Sec 2 we demonstrate the existence of a sonic horizon present for a moving observer due to a modulation of the speed of sound in a piezoelectric substrate, and describe how such a modulation can be achieved using a biased gate. In Sec 3 we

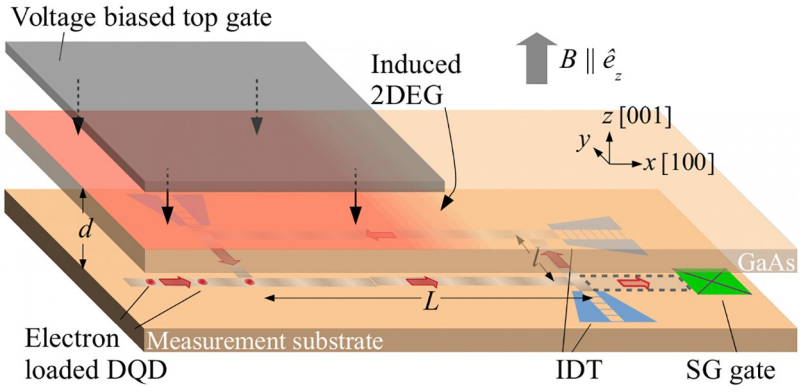

Fig 1. Partial sketch of the experimental set-up. The formation of the sonic horizon for surface acoustic waves on the upper GaAs layer is due to the inhomogeneous two-dimensional electron gas (2DEG) induced by the attached gate. The electrons in the dynamic quantum dots (DQDs) on the lower GaAs layer serve as detector for the created particles in form of piezoelectric phonons: The thermal occupation of the two electron-spin states in the DQDs is expected to be altered due to their spin-orbit interaction with the created phonons. A Stern-Gerlach (SG) gate allows for the readout of the electronic spin. The arrangement of the interdigitated transducers (IDTs) serves as a storage ring for the DQDs in order to provide enough time for interaction. Not shown is the cryogenics.

https://doi.org/10.1371/journal.pone.0229382.g001

describe a measurement set-up using dynamic quantum dots and argue that they equilibrate to a non-thermal state when in contact with a zero-temperature phonon bath. This is attributed to particle creation in form of piezoelectric phonons. In Sec 4 we present concluding remarks.

2 Building blocks

In this section, we will describe the fundamental requirements to generate a sonic horizon for SAWs. In adapting the original proposal of Ref [9] to solid-state devices, the difficulty lies in designing a moving medium for wave propagation. This can be circumvented by having a space- (and time-) dependent wave speed $c(x, t)$. An observer moving with a proper speed v along the waves will eventually experience the crossover between subsonic and supersonic propagation—a direct route for the formation of a sonic horizon. Consequently, this opens up the necessity of a moving detector for measuring the created phonons. Here, the local modulation of the SAW speed can be achieved by exploiting its dependence on the substrate conductivity [32, 41–45], which can be changed locally by biasing a thin gate attached to the piezoelectric p-type semiconducting substrate (see, e.g. Ref [40]): Biasing the gate with a voltage induces a 2DEG in the surface of the substrate in the vicinity to the gate, changing the substrate conductivity. A properly moving detector experiences a sonic horizon for SAWs. The detector comprises of dynamic quantum dots (DQDs) transporting photogenerated electrons and propagating in an adjacent substrate (labeled as measurement substrate in Fig 1). A magnetic field along the [001] axis leads to a Zeeman-splitting of the electron-spin states. Due to spin-orbit interaction between the electrons and the created piezoelectric phonons, the thermal occupation among the spin states is expected to be altered and can be read out by a Stern-Gerlach (SG) gate [38, 46], which converts spin into current paths via the Stern-Gerlach effect. The arrangement of interdigitated transducers (IDTs) serves as storage ring for the electrons and enables for a sufficiently long interaction time required for equilibration (estimated to $\sim$ 1 s, see Sec 3).

We will now derive the effective metric and present set-up details.

2.1 Effective metric

We consider the 1-dimensional propagation of SAWs along the x-direction with a space-dependent speed of sound $c(x)$. With u denoting the SAW amplitude, the dynamics follows the usual wave equation (see, e.g. [47]) [48]

$$\frac{\partial^2 u}{\partial^2 t} = \frac{\partial}{\partial x}\left(c^2(x)\frac{\partial u}{\partial x}\right). \tag{3}$$

This equation describes wave propagation in a space-time with line element given by

$$\mathrm{d}s^2 = -c^2(x)\mathrm{d}t^2 + \mathrm{d}x^2. \tag{4}$$

The Galilean transformation to the reference frame of an observer moving at speed v along the x-direction is accomplished by the substitutions

$$t \to t \quad , \quad x \to x + vt \tag{5}$$

$$\frac{\partial}{\partial t} \to \frac{\partial}{\partial t} - v\frac{\partial}{\partial x} \quad , \quad \frac{\partial}{\partial x} \to \frac{\partial}{\partial x} \tag{6}$$

in Eq 3. Note that c is now a function of x and t. The effective metric describing the SAW

dynamics in the moving reference frame leads to the line element

$$\mathrm{d}s^2 = -[c^2(x - vt) - v^2]\mathrm{d}t^2 + 2v\mathrm{d}t\mathrm{d}x + \mathrm{d}x^2, \tag{7}$$

revealing a sonic horizon where $c^2 - v^2 = 0$. Note that the wave equation and the associated effective metric are given in the rest frame of the substrate. In this coordinate system the effective metric is (only) space-dependent stemming from the space dependence of the speed of sound. The Galilean boost into the frame of the DQDs introduces the time-dependence in the new coordinate system.

This effective metric has features in common with Painlevé-Gullstrand's metric and the Friedmann-Lemaître-Robertson-Walker metric revealing its potential for particle creation, which is supported by calculations using the Bloch-Redfield equations in Sec 3. However, we note that the present set-up does not strictly simulate either of both systems, as Eq 7 does not match their respective metric precisely.

2.2 SAW dynamics

The propagation of SAWs can be controlled by their interaction with a 2DEG in the substrate [32, 41–45]. Here we follow Ref [44], which presents a detailed calculation of SAW propagation on a piezoelectric semiconductor with a *homogeneous* electron gas, and extend their results to the inhomogeneous case.

Due to the piezoelectric effect the SAW is accompanied by an electric field, thus interacting with the 2DEG and inducing currents that dissipate energy due to Ohmic losses. The piezoelectric effect is taken into account by introducing a space dependent charge density n_s that obeys Maxwell's equation

$$\frac{\partial D}{\partial x} = -qn_s \tag{8}$$

in one dimension with the elementary charge denoted by $q = |q|$ (e will be reserved for the piezoelectric constant) and where D is the electric displacement field. The induced current density is given by

$$j(x,t) = -q[n_{2\mathrm{DEG}}(x) + fn_s(x,t)]\mu E(x,t), \tag{9}$$

where μ denotes the electron mobility, f accounts for the part of the induced space charge being in the conduction band (for a calculation of f, see [44]), $n_{2\mathrm{DEG}}$ denotes the *time-independent* density of the 2DEG induced by an attached gate and $E(x, t)$ is the electric field. The time-independence of $n_{2\mathrm{DEG}}$ is necessary in order to recover the usual wave equation for the SAW amplitude. Diffusion currents $\sim k_B T \frac{\partial}{\partial x}(n_{2\mathrm{DEG}} + fn_s)$ due to spatial inhomogeneous charge distribution can be neglected in the low-temperature limit we propose to work in. The total charge density contributing to the electric current is given by

$$\rho = -q[n_{2\mathrm{DEG}} + fn_S]. \tag{10}$$

Using the continuity equation for the charge current and density

$$\frac{\partial \rho}{\partial t} + \frac{\partial j}{\partial x} = 0 \tag{11}$$

and the time-independence of $n_{2\mathrm{DEG}}$, one can derive an equation relating D and E,

$$-\frac{\partial^2 D}{\partial x \partial t} = \mu \frac{\partial}{\partial x}\left(\left[f\frac{\partial D}{\partial x} - qn_{2\mathrm{DEG}}\right]E\right). \tag{12}$$

Using a plane-wave ansatz

$$E = E_0 \exp\{\mathrm{i}(k(x) - \omega t)\} \tag{13}$$

$$D = D_0 \exp\{\mathrm{i}(k(x) - \omega t)\}, \tag{14}$$

and neglecting terms with the product $E \cdot D$ [49], one can write $D = \varepsilon_{\mathrm{eff}} E$ with an effective permittivity

$$\varepsilon_{\mathrm{eff}} = \frac{\mu q}{\omega}\left[\frac{\partial_x n_{\mathrm{2DEG}}}{\partial_x k} + \mathrm{i} n_{\mathrm{2DEG}}\right], \tag{15}$$

where ∂_x abbreviates the spatial derivative. The equations of state for a piezoelectric material

$$T = dS - eE \tag{16}$$

$$D = eS + \varepsilon E, \tag{17}$$

where T and S denote stress and strain constants, d is the elastic constant and e is the piezoelectric constant, can be simplified to $T = d_{\mathrm{eff}} S$ with an effective elastic constant

$$d_{\mathrm{eff}} = d\left[1 + \frac{e^2}{\varepsilon d}\left(1 - \frac{\varepsilon_{\mathrm{eff}}}{\varepsilon}\right)^{-1}\right]. \tag{18}$$

This equation illustrates the effect of piezoelectric stiffening, i.e. a dressed elastic constant due to the piezoelectric effect [50]. The equation of motion for the SAW amplitude u is given by

$$S = \frac{\partial u}{\partial x} \text{ and } \frac{\partial T}{\partial x} = \rho \frac{\partial^2 u}{\partial t^2}, \tag{19}$$

leading, with Eq 18, finally to the wave equation of Eq 3 with the SAW speed given by

$$c(x) = \mathrm{Re}\left(\sqrt{\frac{\mathrm{d}_{\mathrm{eff}}}{\rho}}\right). \tag{20}$$

Note that the RHS of Eq 20 also depends on the SAW speed via $\partial_x k(x) = \omega / c(x)$. Thus, solving Eq 20 for $c(x)$ gives, in principle, an expression for the SAW speed in terms of the 2DEG density. An approximate solution is given in S1 Appendix.

2.3 2DEG density modulation

In this section we describe the charge distribution in the 2DEG which is induced by the attached gate biased with a voltage $V_G \sim 10$ V. As a bare approximation the 2DEG is assumed to distribute homogeneously over the area of the gate,

$$n_0(x) = n_{\mathrm{max}} H(-x)\ , \tag{21}$$

with a density amplitude n_{max} proportional to the applied gate voltage V_G [40], and the Heaviside step function $H(x)$. However, the actual 2DEG is smeared out and its density n_{2DEG} is smoothed close to the gate's edge (illustrated in Fig 2). We take this into account by

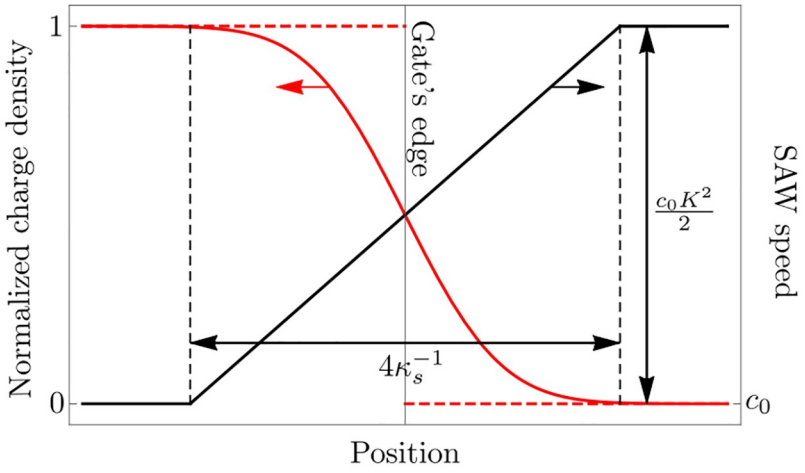

Fig 2. Spatial profiles around the gate's edge. Shown are the densities of the approximate (dashed red) and actual, smeared out (solid red) charge distribution of the induced 2DEG. The latter one arises from the first one due to screening effects inside the semiconducting substrate, which smoothen the charge density in a narrow region of approximate thickness $4\kappa_s^{-1}$ around the gate's edge with the screening length κ_s^{-1}. The corresponding SAW speed $c(x)$ (black) according to Eq 20 takes the values c_0 and $c_0(1 + K^2/2)$ with the piezoelectric coupling constant K^2 in the region with high and low 2DEG density, respectively, and approximately aligns linearly in the transition region.

https://doi.org/10.1371/journal.pone.0229382.g002

convoluting the approximated density $n_0(x)$ and a Gaussian with FWHM denoted by κ_s^{-1}, reading

$$G(x) = A \exp\left[-(\kappa_s x)^2\right], \tag{22}$$

$$n_{2\mathrm{DEG}}(x) = (G * n_0)(x) \tag{23}$$

$$= \frac{n_{\max}}{2}\left[1 - \mathrm{erf}(\kappa_s x)\right], \tag{24}$$

where "$*$" denotes the convolution operation. The normalization coefficient A guarantees charge conservation,

$$\int_{-\infty}^{\infty} [n_{2\mathrm{DEG}}(x) - n_0(x)]\mathrm{d}x = 0. \tag{25}$$

The phenomenological parameter κ_s^{-1} should be of the order of the screening length of the substrate material which, for moderate doping of the p-type semiconducting substrate, is typically of the order of 10^{-8} m [51, 52]. This is the density that will modulate the speed of sound for the SAWs in Eq 20.

3 Particle creation and detection

The comparison of the two effective metrics with line elements Eqs 7 and 4 shows that a sonic horizon is present only in the reference frame of the moving observer. Consequently, particle creation is expected to occur and to be measured only in the moving reference frame as well. This is a result of the observer dependent notion of particles (see, e.g. [53]) [54]. For this purpose, we propose to use moving electrons trapped in the lateral piezoelectric potentials accompanying SAWs, also known as dynamic quantum dots (DQDs), as proposed in [55, 56]. The

DQDs move on the measurement substrate, so that their speed v is constant and does not follow the speed profile $c(x)$ of the upper substrate (see Fig 1). In this section we show that the DQDs reach a non-thermal steady-state, even when interacting with a zero-temperature phononic bath, which we argue is due to the particle creation in the moving frame.

We choose a coordinate system with axes x and z pointing along the [100] and [001] axes of GaAs. Applying a magnetic field $B \sim 1$ T [57, 58] along the z axis leads to Zeeman-splitting of the two electron-spin states denoted by $|\uparrow\rangle$ and $|\downarrow\rangle$, respectively, with an energy separation $E_\uparrow - E_\downarrow = E_0 = g\mu_B B$. The Dresselhaus spin-orbit coupling [59] is the dominant process for spin-flip transitions between the Zeemann sublevels in the DQD [56, 60].

For a motion of the DQD in x direction, $\mathbf{v} = v\hat{e}_x$, the Hamiltonian approximately describing the electron-spin while interacting with the piezoelectric phonons can be written as $H = H_S + H_{\mathrm{SB}} + H_B$ with the spin Hamiltonian [61–66]

$$H_S = E_0\sigma_z + \Delta E\sigma_y, \tag{26}$$

the phonon bath Hamiltonian

$$H_B = \sum_q \hbar\omega_q \left(b_q^\dagger b_q + \frac{1}{2}\right) \tag{27}$$

and their mutual interaction Hamiltonian

$$H_{\mathrm{SB}} = \sigma_x \sum_q M_q \mathrm{e}^{\mathrm{i}qvt}(b_{-q}^\dagger + b_q). \tag{28}$$

Here, ΔE originates from a motion induced constant magnetic field, and the spin-phonon coupling is due to a motion induced magnetic noise originating from the electric noise due to the piezophonons [61, 62]. Details about the parameters and their dependence on the DQD speed and the material constants can be found in Ref [61] and references therein. Using this model Hamiltonian, the dynamics of the DQD spin while interacting with the phonon system can be calculated using the Bloch-Redfield equations, which read [67]

$$\dot{\rho}_{\mu\nu}(t) = -\mathrm{i}\omega_{\mu\nu}\rho_{\mu\nu}(t) + \sum_{\kappa\lambda} R_{\mu\nu\kappa\lambda}\rho_{\kappa\lambda}(t). \tag{29}$$

Here, $R_{\mu\nu\kappa\lambda}$ are the elements of the Redfield tensor and the $\rho_{\mu\nu}$ are the elements of the reduced density matrix of the DQD in the eigenstate basis of H_S denoted by $|0\rangle$ and $|1\rangle$ for the ground and excited state, respectively. For eigenstates $|\mu\rangle$ and $|\nu\rangle$ of H_S with eigenenergies E_μ and E_ν, respectively, $\omega_{\mu\nu}$ is defined as $\omega_{\mu\nu} = (E_\mu - E_\nu)/\hbar$. The Redfield tensor has the form [67, 68]

$$R_{\mu\nu\kappa\lambda} = \Gamma^+_{\lambda\nu\mu\kappa} + \Gamma^-_{\lambda\nu\mu\kappa} - \delta_{\nu\lambda}\sum_\alpha \Gamma^+_{\mu\alpha\alpha\kappa} - \delta_{\mu\kappa}\sum_\alpha \Gamma^-_{\lambda\alpha\alpha\nu} \tag{30}$$

with the rates given by [67, 68]

$$\Gamma^+_{\lambda\nu\mu\kappa} = \hbar^{-2}\int_0^\infty \mathrm{d}t \langle\langle\lambda|H_{I,\mathrm{SB}}(t)|\nu\rangle\langle\mu|H_{I,\mathrm{SB}}(0)|\kappa\rangle\rangle_{\mathrm{bath}} \mathrm{e}^{-\mathrm{i}\omega_{\mu\kappa}t} \tag{31}$$

$$\Gamma^-_{\lambda\nu\mu\kappa} = \hbar^{-2}\int_0^\infty \mathrm{d}t \langle\langle\lambda|H_{I,\mathrm{SB}}(0)|\nu\rangle\langle\mu|H_{I,\mathrm{SB}}(t)|\kappa\rangle\rangle_{\mathrm{bath}} \mathrm{e}^{-\mathrm{i}\omega_{\lambda\nu}t}, \tag{32}$$

where $\langle\cdot\rangle_{\mathrm{bath}}$ is the expectation value of the bath observable and $H_{I,\mathrm{SB}}$ is the interaction

Hamiltonian in the interaction picture with respect to the bath Hamiltonian,

$$H_{I,\mathrm{SB}}(t) = \exp\{\mathrm{i}H_B t/\hbar\} H_{\mathrm{SB}} \exp\{-\mathrm{i}H_B t/\hbar\} \tag{33}$$

$$= \sigma_x \sum_q M_q \mathrm{e}^{\mathrm{i}qvt}(b^\dagger_{-q}\mathrm{e}^{\mathrm{i}\omega_q t} + b_q \mathrm{e}^{-\mathrm{i}\omega_q t}). \tag{34}$$

Using $\langle b^\dagger_{-q} b_l\rangle = \delta_{-q,l} n(\omega_q)$ with the Bose-Einstein distribution $n(\omega)$ the rates can be expressed as

$$\Gamma^+_{\lambda\nu\mu\kappa} = M_{\lambda\nu\mu\kappa} \sum_q |M_q|^2 \int_0^\infty \mathrm{d}t \{\mathrm{e}^{\mathrm{i}[qv+\omega_q-\omega_{\mu\kappa}]t} n(\omega_q) + \mathrm{e}^{\mathrm{i}[qv-\omega_q-\omega_{\mu\kappa}]t}(n(\omega_q)+1)\} \tag{35}$$

$$\Gamma^-_{\lambda\nu\mu\kappa} = M_{\lambda\nu\mu\kappa} \sum_q |M_q|^2 \int_0^\infty \mathrm{d}t \{\mathrm{e}^{\mathrm{i}[qv-\omega_q-\omega_{\lambda\nu}]t} n(\omega_q) + \mathrm{e}^{\mathrm{i}[qv+\omega_q-\omega_{\lambda\nu}]t}(n(\omega_q)+1)\}, \tag{36}$$

where $M_{\lambda\nu\mu\kappa} = \hbar^{-2}\langle\lambda|\sigma_x|\nu\rangle\langle\mu|\sigma_x|\kappa\rangle$.

For a subsonic motion, $v < c$, these rates are given by

$$\Gamma^+_{\lambda\nu\mu\kappa} = \frac{\pi}{2} M_{\lambda\nu\mu\kappa} \begin{cases} \frac{J(\omega^-_{\kappa\mu})}{1-v/c}\left[n\left(\omega^-_{\kappa\mu}\right)+1\right] + \frac{J(\omega^+_{\kappa\mu})}{1+v/c}\left[n\left(\omega^+_{\kappa\mu}\right)+1\right] & ,\omega_{\kappa\mu}>0 \\ \frac{J(\omega^+_{\mu\kappa})}{1+v/c} n\left(\omega^+_{\mu\kappa}\right) + \frac{J(\omega^-_{\mu\kappa})}{1-v/c} n\left(\omega^-_{\mu\kappa}\right) & ,\omega_{\mu\kappa}>0 \end{cases} \tag{37}$$

$$\Gamma^-_{\lambda\nu\mu\kappa} = \frac{\pi}{2} M_{\lambda\nu\mu\kappa} \begin{cases} \frac{J(\omega^-_{\lambda\nu})}{1-v/c}\left[n\left(\omega^-_{\lambda\nu}\right)+1\right] + \frac{J(\omega^+_{\lambda\nu})}{1+v/c}\left[n\left(\omega^+_{\lambda\nu}\right)+1\right] & ,\omega_{\lambda\nu}>0 \\ \frac{J(\omega^+_{\nu\lambda})}{1+v/c} n\left(\omega^+_{\nu\lambda}\right) + \frac{J(\omega^-_{\nu\lambda})}{1-v/c} n\left(\omega^-_{\nu\lambda}\right) & ,\omega_{\nu\lambda}>0 \end{cases}, \tag{38}$$

with $\omega^\pm_{\alpha\beta} = \omega_{\alpha\beta}/(1\pm v/c)$ and where $J(\omega) = \sum_q |M_q|^2 \delta(\omega-\omega_q)$ denotes the spectral density and it was used that $\int_0^\infty \mathrm{e}^{\mathrm{i}\omega t}\mathrm{d}t = \pi\delta(\omega)$, where the imaginary parts resulting from principal value integrals are neglected as they manifest themselves as Lamb shifts.

For a supersonic motion, $v > c$, and a vanishing temperature of the phonon bath, the rates are given by

$$\Gamma^+_{\lambda\nu\mu\kappa} = \frac{\pi}{2} M_{\lambda\nu\mu\kappa} \begin{cases} \frac{J(\omega^+_{\kappa\mu})}{v/c+1} & ,\omega_{\kappa\mu}>0 \\ \frac{J(\omega^-_{\mu\kappa})}{v/c-1} & ,\omega_{\mu\kappa}>0 \end{cases} \tag{39}$$

$$\Gamma^-_{\lambda\nu\mu\kappa} = \frac{\pi}{2} M_{\lambda\nu\mu\kappa} \begin{cases} \frac{J(\omega^+_{\lambda\nu})}{v/c+1} & ,\omega_{\lambda\nu}>0 \\ \frac{J(\omega^-_{\nu\lambda})}{v/c-1} & ,\omega_{\nu\lambda}>0 \end{cases}. \tag{40}$$

From Eqs 37, 38, 39 and 40, respectively, the Redfield tensor Eq 30 can be computed for each corresponding case.

For the steady state solution of the Bloch-Redfield Eq 29 one finds vanishing off-diagonal matrix elements, $\rho_{10} = \rho_{01} = 0$, in both sub- and supersonic cases, as expected due to spin

decoherence. The diagonal matrix elements can be expressed as

$$\frac{\rho_{11}}{\rho_{00}} = \frac{\Gamma_{12}}{\Gamma_{21}} \tag{41}$$

with the absorption rate $\Gamma_{12} = R_{1111} = \Gamma^{+}_{1221} + \Gamma^{-}_{1221}$ and the emission rate $\Gamma_{21} = R_{1122} = \Gamma^{+}_{2112} + \Gamma^{-}_{2112}$.

For subsonic motion, $v < c$, these rates explicitly read

$$\Gamma_{12} = \frac{\pi}{2} M_{1221} \left\{ \frac{J(\omega^{+}_{21})}{1 + v/c} n(\omega^{+}_{21}) + \frac{J(\omega^{-}_{21})}{1 - v/c} n(\omega^{-}_{21}) \right\} \tag{42}$$

$$\Gamma_{21} = \frac{\pi}{2} M_{1221} \left\{ \frac{J(\omega^{+}_{21})}{1 + v/c} \left[n(\omega^{+}_{21}) + 1 \right] + \frac{J(\omega^{-}_{21})}{1 - v/c} \left[n(\omega^{-}_{21}) + 1 \right] \right\}. \tag{43}$$

The steady state Eq 41 is clearly non-thermal in the sense that the effective temperature T' of the DQD, given via

$$\frac{\rho_{11}}{\rho_{00}} = \exp\left(-\frac{\hbar \omega_{10}}{k_B T'} \right), \tag{44}$$

does not in general coincide with the temperature of the phonon bath the DQD is in contact with, $T \neq T'$. In this scenario the rates and thus the non-thermality can be easily explained via the Doppler-effect: Phonons participating in transitions in the DQD have a frequency in the rage $\Omega = [\omega_{10} - \Delta\omega/2, \omega_{10} + \Delta\omega/2]$ with the line width $\Delta\omega$. As these frequencies are measured in the reference frame of the DQD, and the speed of sound c and the speed of the DQD add up/subtract leading to a Doppler-shift $\omega \to (1 \pm v/c)\omega$, there are in fact two frequency ranges involved in transitions, namely $\Omega/(1 \pm v/c)$ measured in the bath frame. Each of them contribute to the absorption and emission rate in the usual manner, where the prefactors $(1 \pm v/c)^{-1}$ are due to the Doppler-shifted line width. Furthermore, for a zero temperature phonon bath the absorption rate also vanishes, $\Gamma_{12} = 0$, since there are no phonons present which could excite the DQD and thus the DQD equilibrates with the phonon bath by relaxing to its ground state and thus having vanishing effective temperature.

In the case of supersonic motion, $v > c$, where we restricted the analyses to a vanishing bath temperature $T = 0$, the absorption and emission rates are now given by

$$\Gamma_{12} = \pi \frac{M_{1221}}{v/c - 1} J(\omega^{-}_{21}) \tag{45}$$

$$\Gamma_{21} = \pi \frac{M_{1221}}{v/c + 1} J(\omega^{+}_{21}). \tag{46}$$

Even though the bath is at zero temperature, the effective temperature of the DQD given via Eq 44 is non-vanishing, because the absorption rate does not vanish. We argue that this motion-enhanced character of the density matrix can be attributed to the presence of excess particles in form of piezophonons originating from particle creation, which excite the DQD and lead it to a steady state which is not in thermal equilibrium with the bath.

The use of Stern-Gerlach gates or other spin-to-charge conversion methods allows for the readout of the electron spin from which the effective DQD temperature can be computed. Equilibration is expected to be achieved after a time $\Gamma_{12} + \Gamma_{21}$ (see, e.g. [69]), where the Γ-

terms denote the rate for a spin-flip with emission and absorption of a piezophonon, respectively. An upper bound for the equilibration time is given by the rate for spontaneous emission of a piezophonon. A rough estimation of this rate for the present set-up is given by Eq (8) of Ref [60], but with an additional factor exp $\{-2d(g\mu_B B)/(\hbar c)\}$, where d denotes the distance between the two substrates, taking into account the exponential decay of the piezoelectric field accompanying the piezophonons [32, 70], and the energy conservation, $\hbar ck = g\mu_B B$ [71–74]. For a magnetic field $B = 1$ T, the equilibration rate is of the order of 1 s^{-1}. The steady state of the electron spin could be achieved while the electrons are stored in a storage ring as it is shown in Fig 1. Efficient electron transport over macroscopic distances has been shown in [75]: The lengths l, L of the storage ring can be chosen arbitrarily in the sub-mm regime. Future conveyor belts for electrons using serpentine-shaped SAW waveguides [76, 77] could provide an alternate route to reach equilibration. In comparison, however, the present set-up details make the proposed storage ring more feasible.

We note that the use of quantum field theory for the SAW field whose propagation is described by the metrics with line elements given in Eqs 4 and 7, respectively, is a more natural route to study particle creation in this system. A Bogoliubov transformation can be computed from the two sets of positive and negative frequency modes used for the reference frame of the substrate and the moving observer, respectively. Particle creation occurs if positive (or negative) frequency modes from one set appears as mixture of both positive and negative frequency modes from the other set. We do not use this approach as it is out of scope of the present study and leave it for future work.

4 Conclusion

We have presented a new semiconductor analogue system to simulate quantum effects in general relativity. Particle creation in this system is expected for a DQD moving with constant speed in the measurement substrate. The detailed steps to achieve this are discussed, including the charge density modulation of a two dimensional electron gas which is responsible for the change in speed of sound for SAWs travelling on the substrate. This in turn leads to a sonic horizon for SAWs seen by the DQD.

We analyzed a measurement scheme to detect the created particles using the DQDs, whose steady-state spin populations differ from that of a thermal state due to their interaction with the created piezophonons. We stress that a number of different alternatives to observe the evanescent waves could be pursued, as their detection is well developed in fields such as biosensing [78]. However, these schemes must be adapted to allow for the characterization of the quantum nature of the associated SAW phonons.

We note that the origin of the excess phonons in the moving frame is not clear. Further work to determine the cosmological nature of this radiation is still required.

Supporting information

S1 Appendix. Approximation of the SAW speed.
(PDF)

Acknowledgments

We thank Malte Henkel, Rodrigo Turcati, David Edward Bruschi and specially Germain Rousseaux for helpful discussions. The authors would like to acknowledge the reviewers for pointing out important issues that lead to significant improvement of this work.

Author Contributions

Conceptualization: Frank K. Wilhelm.

Funding acquisition: Frank K. Wilhelm.

Investigation: Raphael P. Schmit, Bruno G. Taketani.

Project administration: Frank K. Wilhelm.

Writing – original draft: Raphael P. Schmit, Bruno G. Taketani, Frank K. Wilhelm.

References

1. Greiner W, Schramm S. Resource letter QEDV-1: the QED vacuum. American Journal of Physics. 2008; 76(6):509–518. https://doi.org/10.1119/1.2820395
2. Scully MO, Zubairy MS. Quantum optics. Cambridge University Press. 1997
3. Yablonovitch E. Accelerating reference frame for electromagnetic waves in a rapidly growing plasma: Unruh-Davies-Fulling-DeWitt radiation and the nonadiabatic Casimir effect. Physical Review Letters. 1989; 62(15):1742. https://doi.org/10.1103/PhysRevLett.62.1742 PMID: 10039756
4. Schwinger J. Casimir energy for dielectrics. Proceedings of the National Academy of Sciences of the United States of America. 1992; 89(9):4091. https://doi.org/10.1073/pnas.89.9.4091 PMID: 11607291
5. Bruschi DE, Fuentes I, Louko J. Voyage to Alpha Centauri: Entanglement degradation of cavity modes due to motion. Physical Review D. 2012; 85(6);061701. https://doi.org/10.1103/PhysRevD.85.061701
6. Parker L. Particle creation in expanding universes. Physical Review Letters. 1968; 21(8):562. https://doi.org/10.1103/PhysRevLett.21.562
7. Hawking SW. Particle creation by black holes. Communications in Mathematical Physics. 1975; 43(3):199–220. https://doi.org/10.1007/BF02345020
8. Wilson CM, Johansson G, Pourkabirian A, Simoen M, Johansson JR, Duty T, et al. Observation of the dynamical Casimir effect in a superconducting circuit. Nature. 2011; 479(7373):376. https://doi.org/10.1038/nature10561 PMID: 22094697
9. Unruh WG. Experimental black-hole evaporation? Physical Review Letters. 1981; 46(21):1351. https://doi.org/10.1103/PhysRevLett.46.1351
10. Painlevé P. Le Mecanique Classique et la Theorie de la Relativite. L'Astronomie. 1922; 36:6–9.
11. Fedichev PO, Fischer UR. Gibbons-Hawking effect in the sonic de Sitter space-time of an expanding Bose-Einstein-condensed gas. Physical review letters. 2003; 91(24):240407. https://doi.org/10.1103/PhysRevLett.91.240407 PMID: 14683099
12. Fischer UR, Schützhold R. Quantum simulation of cosmic inflation in two-component Bose-Einstein condensates. Physical Review A. 2004; 70(6):063615. https://doi.org/10.1103/PhysRevA.70.063615
13. Eckel S, Kumar A, Jacobson T, Spielman IB, Campbell GK. A rapidly expanding Bose-Einstein condensate: an expanding universe in the lab. Physical Review X. 2018; 8(2):021021. https://doi.org/10.1103/PhysRevX.8.021021
14. Fey C, Schaetz T, Schützhold R. Ion-trap analog of particle creation in cosmology. Physical Review A. 2018; 98(3):033407. https://doi.org/10.1103/PhysRevA.98.033407
15. Wittemer M, Hakelberg F, Kiefer P, Schröder JP, Fey C, Schützhold R. Particle pair creation by inflation of quantum vacuum fluctuations in an ion trap. arXiv preprint arXiv:190305523. 2019.
16. Jacobson T, Volovik G. Event horizons and ergoregions in 3 He. Physical Review D. 1998; 58 (6):064021. https://doi.org/10.1103/PhysRevD.58.064021
17. Nation P, Blencowe M, Rimberg A, Buks E. Analogue Hawking radiation in a dc-SQUID array transmission line. Physical Review Letters. 2009; 103(8):087004. https://doi.org/10.1103/PhysRevLett.103.087004 PMID: 19792751
18. Schützhold R, Unruh WG. Hawking radiation in an electromagnetic waveguide? Physical Review Letters. 2005; 95(3):031301. https://doi.org/10.1103/PhysRevLett.95.031301 PMID: 16090733
19. Rousseaux G, Mathis C, Maïssa P, Philbin TG, Leonhardt U. Observation of negative-frequency waves in a water tank: a classical analogue to the Hawking effect? New Journal of Physics. 2008; 10 (5):053015. https://doi.org/10.1088/1367-2630/10/5/053015
20. Weinfurtner S, Tedford EW, Penrice MCJ, Unruh WG, Lawrence GA. Measurement of Stimulated Hawking Emission in an Analogue System. Physical Review Letters. 2011; 106:021302. https://doi.org/10.1103/PhysRevLett.106.021302 PMID: 21405217

21. Euvé LP, Michel F, Parentani R, Philbin T, Rousseaux G. Observation of noise correlated by the Hawking effect in a water tank. Physical Review Letters. 2016; 117(12):121301. https://doi.org/10.1103/PhysRevLett.117.121301 PMID: 27689260

22. Nguyen H, Gerace D, Carusotto I, Sanvitto D, Galopin E, Lemaître A et. al. Acoustic black hole in a stationary hydrodynamic flow of microcavity polaritons. Physical Review Letters. 2015; 114(3):036402. https://doi.org/10.1103/PhysRevLett.114.036402 PMID: 25659010

23. Elazar M, Fleurov V, Bar-Ad S. All-optical event horizon in an optical analog of a Laval nozzle. Physical Review A. 2012; 86(6):063821. https://doi.org/10.1103/PhysRevA.86.063821

24. Philbin TG, Kuklewicz C, Robertson S, Hill S, König F, Leonhardt U. Fiber-optical analog of the event horizon. Science. 2008; 319(5868):1367–1370. https://doi.org/10.1126/science.1153625 PMID: 18323448

25. Marino F. Acoustic black holes in a two-dimensional "photon fluid". Physical Review A. 2008; 78 (6):063804. https://doi.org/10.1103/PhysRevA.78.063804

26. Belgiorno F, Cacciatori SL, Clerici M, Gorini V, Ortenzi G, Rizzi L, et al. Hawking radiation from ultrashort laser pulse filaments. Physical review letters. 2010; 105(20):203901. https://doi.org/10.1103/PhysRevLett.105.203901 PMID: 21231233

27. Steinhauer J. Observation of quantum Hawking radiation and its entanglement in an analogue black hole. Nature Physics. 2016; 12(10):959. https://doi.org/10.1038/nphys3863

28. Cropp B, Liberati S, Turcati R. Analogue black holes in relativistic BECs: Mimicking Killing and universal horizons. Physical Review D. 2016; 94(6):063003. https://doi.org/10.1103/PhysRevD.94.063003

29. Lange K, Peise J, Lücke B, Gruber T, Sala A, Polls A, et al. Creation of entangled atomic states by an analogue of the Dynamical Casimir effect. New Journal of Physics. 2018; 20(10):103017. https://doi.org/10.1088/1367-2630/aae116

30. Vezzoli S, Mussot A, Westerberg N, Kudlinski A, Saleh HD, Prain A, et al. Optical Analogue of the Dynamical Casimir Effect in a Dispersion-Oscillating Fibre. Communications Physics. 2019; 2(84).

31. Schützhold R, Uhlmann M, Petersen L, Schmitz H, Friedenauer A, Schätz T. Analogue of cosmological particle creation in an ion trap. Physical Review Letters. 2007; 99(20):201301. https://doi.org/10.1103/PhysRevLett.99.201301 PMID: 18233131

32. Simon SH. Coupling of surface acoustic waves to a two-dimensional electron gas. Physical Review B. 1996; 54(19):13878. https://doi.org/10.1103/PhysRevB.54.13878

33. Rahman S, Kataoka M, Barnes CHW, Langtangen HP. Numerical investigation of a piezoelectric surface acoustic wave interaction with a one-dimensional channel. Physical Review B. 2006; 74:035308. https://doi.org/10.1103/PhysRevB.74.035308

34. Shao L, Pipe KP. Amplification and directional emission of surface acoustic waves by a two-dimensional electron gas. Applied Physics Letters. 2015; 106(2):023106. https://doi.org/10.1063/1.4905836

35. Efros AL, Galperin YM. Quantization of the acoustoelectric current in a two-dimensional electron system in a strong magnetic field. Physical Review Letters. 1990; 64:1959–1962. https://doi.org/10.1103/PhysRevLett.64.1959 PMID: 10041538

36. McNeil RPG, Kataoka M, Ford CJB, Barnes CHW, Anderson D, Jones GAC, et al. On-demand single-electron transfer between distant quantum dots. Nature. 2011; 477(7365):439–442. https://doi.org/10.1038/nature10444 PMID: 21938065

37. Hermelin S, Takada S, Yamamoto M, Tarucha S, Wieck AD, Saminadayar L, et al. Electrons surfing on a sound wave as a platform for quantum optics with flying electrons. Nature. 2011; 477(7365):435–438. https://doi.org/10.1038/nature10416 PMID: 21938064

38. Barnes C, Shilton J, Robinson A. Quantum computation using electrons trapped by surface acoustic waves. Physical Review B. 2000; 62(12):8410. https://doi.org/10.1103/PhysRevB.62.8410

39. Gustafsson MV, Aref T, Kockum AF, Ekström MK, Johansson G, Delsing P. Propagating phonons coupled to an artificial atom. Science. 2014; 346(6206):207–211. https://doi.org/10.1126/science.1257219 PMID: 25213379

40. Sze SM. Semiconductor Devices: Physics and Technology. John Wiley & Sons; 2008.

41. Ingebrigtsen K. Linear and nonlinear attenuation of acoustic surface waves in a piezoelectric coated with a semiconducting film. Journal of Applied Physics. 1970; 41(2):454–459. https://doi.org/10.1063/1.1658696

42. Gumbs G, Aizin G, Pepper M. Interaction of surface acoustic waves with a narrow electron channel in a piezoelectric material. Physical Review B. 1998; 57(3):1654. https://doi.org/10.1103/PhysRevB.57.1654

43. Bierbaum P. Interaction of ultrasonic surface waves with conduction electrons in thin metal films. Applied Physics Letters. 1972; 21(12):595–598. https://doi.org/10.1063/1.1654269

44. Hutson A, White DL. Elastic wave propagation in piezoelectric semiconductors. Journal of Applied Physics. 1962; 33(1):40–47. https://doi.org/10.1063/1.1728525

45. Wixforth A, Scriba J, Wassermeier M, Kotthaus J, Weimann G, Schlapp W. Surface acoustic waves on GaAs/Al_x Ga_{1-x} As heterostructures. Physical Review B. 1989; 40(11):7874. https://doi.org/10.1103/PhysRevB.40.7874

46. Furuta S, Barnes C, Doran C. Single-qubit gates and measurements in the surface acoustic wave quantum computer. Physical Review B. 2004; 70(20):205320. https://doi.org/10.1103/PhysRevB.70.205320

47. Datta S. Surface acoustic wave devices. Prentice Hall; 1986.

48. The SAW-type solutions (Rayleigh, Lamb and Love waves) are only obtained from the usual wave equation by taking appropriate boundary conditions into account. However, these boundary conditions effectively put constraints on the SAW amplitude and velocity. As a result, the SAW dynamics still follow the usual wave equation, only with the SAW speed differing from the bulk value.

49. Following Ref [44] these terms can be neglected if the strain amplitude $S \ll \varepsilon v/(e\mu) \sim 10^{-6}$ for GaAs. As the upper layer is not driven, the strain amplitude is estimated to be in the 10^{-9}-regime.

50. Johannsmann D. The Quartz Crystal Microbalance in Soft Matter Research. Soft and Biological Matter. 2015; p. 191–204. https://doi.org/10.1007/978-3-319-07836-6_8

51. Mahan GD. Many-particle Physics. Springer Science & Business Media; 2013.

52. Stern F. Low-temperature limit of screening length in semiconductors. Physical Review B. 1974; 9(10):4597. https://doi.org/10.1103/PhysRevB.9.4597

53. Fedichev PO, Fischer UR. Observer dependence for the phonon content of the sound field living on the effective curved space-time background of a Bose-Einstein condensate. Physical Review D. 2004; 69(6):064021. https://doi.org/10.1103/PhysRevD.69.064021

54. In a flat space-time particle creation does not occur for two inertial observers because of the Lorentz invariance. In analogue models, however, the existence of a preferred speed (i.e. speed of sound in the present set-up) breaks Lorentz invariance. The motion of the moving observer can be regarded as an accelerated motion while passing the region where the SAW speed changes locally.

55. Rocke C, Zimmermann S, Wixforth A, Kotthaus J, Böhm G, Weimann G. Acoustically driven storage of light in a quantum well. Physical Review Letters. 1997; 78(21):4099. https://doi.org/10.1103/PhysRevLett.78.4099

56. Stotz J, Alsina F, Hey R, Santos P. Acoustically induced dynamic potential dots. Physica E: Low-dimensional Systems and Nanostructures. 2005; 26(1):67–71. https://doi.org/10.1016/j.physe.2004.08.025

57. For a magnetic field $B \sim 1$ T the effective magnetic field $B_{\text{eff}} \sim 10$ mT associated with Dresselhaus spin-orbit coupling [75] can be treated as a small perturbation.

58. Stotz J, Hey R, Santos P, Ploog K. Coherent spin transport through dynamic quantum dots. Nature materials. 2005; 4(8):585–588. Nature. 2011;477(7365):435–438. https://doi.org/10.1038/nmat1430 PMID: 16041380

59. Dresselhaus G. Spin-orbit coupling effects in zinc blende structures. Physical Review. 1955; 100(2):580. https://doi.org/10.1103/PhysRev.100.580

60. Khaetskii AV, Nazarov YV. Spin-flip transitions between Zeeman sublevels in semiconductor quantum dots. Physical Review B. 2001; 64(12):125316. https://doi.org/10.1103/PhysRevB.64.125316

61. Zhao X, Huang P, Hu X. Doppler effect induced spin relaxation boom. Scientific reports. 2016; 6:23169. https://doi.org/10.1038/srep23169 PMID: 26996253

62. Huang P, Hu X. Spin qubit relaxation in a moving quantum dot. Physical Review B. 2013; 88(7):075301. https://doi.org/10.1103/PhysRevB.88.075301

63. Golovach VN, Khaetskii A, Loss D. Phonon-induced decay of the electron spin in quantum dots. Physical review letters. 2004; 93(1):016601. https://doi.org/10.1103/PhysRevLett.93.016601

64. Borhani M, Golovach VN, Loss D. Spin decay in a quantum dot coupled to a quantum point contact. Physical Review B. 2006; 73(15):155311. https://doi.org/10.1103/PhysRevB.73.155311

65. Golovach VN, Borhani M, Loss D. Electric-dipole-induced spin resonance in quantum dots. Physical Review B. 2006; 74(16):165319. https://doi.org/10.1103/PhysRevB.74.165319

66. Huang P, Hu X. Electron spin relaxation due to charge noise. Physical Review B. 2014; 89(19):195302. https://doi.org/10.1103/PhysRevB.89.195302

67. Weiss U. Quantum dissipative systems. vol. 13. World scientific; 2012.

68. Blum K. Density matrix theory and applications. vol. 64. Springer Science & Business Media; 2012.

69. Breuer HP, Petruccione F. The theory of open quantum systems. Oxford University Press on Demand; 2002.

70. Aizin G, Gumbs G, Pepper M. Screening of the surface-acoustic-wave potential by a metal gate and the quantization of the acoustoelectric current in a narrow channel. Physical Review B. 1998; 58(16):10589. https://doi.org/10.1103/PhysRevB.58.10589

71. The energy separation $\hbar\omega_0$ between the electron orbital states inside the lateral piezoelectric potential is estimated as follows: In the single-electron Hamiltonian given in [46, 72, 73], the SAW-potential term is expanded around its minimum, giving rise to a harmonic oscillator with an excitation energy $\hbar\omega_0 = h/\lambda (U_0/m)^{1/2}$, where λ, $m = 0.067m_e$ and U_0 denote the SAW wavelength, effective electron mass and the SAW-potential strength, respectively. With typical values of $U_0 \sim 40 - 600$ meV [72, 74] and $\lambda = 1\ \mu$m, $\hbar\omega_0$ is in the meV regime, agreeing with numerical results of Ref [73].

72. Robinson A, Barnes C. Classical dynamics of electrons in quantized-acoustoelectric-current devices. Physical Review B. 2001; 63(16):165418. https://doi.org/10.1103/PhysRevB.63.165418

73. Shi X, Zhang M, Wei LF. Quantum computation with moving quantum dots generated by surface acoustic waves. Physical Review A. 2011; 84(6):062310. https://doi.org/10.1103/PhysRevA.84.062310

74. Buitelaar M, Leek P, Talyanskii V, Smith C, Anderson D, Jones G, et al. Charge pumping and current quantization in surface acoustic-wave-driven carbon nanotube devices. Semiconductor Science and Technology. 2006; 21(11):S69. https://doi.org/10.1088/0268-1242/21/11/S10

75. Assuming an exponential decay of the number of charge carriers along the propagation direction, $c(x) \sim \exp(-x/\Lambda)$, the decay constant Λ can be estimated to several thousand SAW wavelengths for Ref [55]. Further increase could be achieved by increasing the SAW power.

76. Boucher P, Rauwerdink S, Tahraoui A, Wenger C, Yamamoto Y, Santos P. Ring waveguides for gigahertz acoustic waves on silicon. Applied Physics Letters. 2014; 105(16):161904. https://doi.org/10.1063/1.4898814

77. Adkins L, Hughes A. Long delay lines employing surface acoustic wave guidance. Journal of Applied Physics. 1971; 42(5):1819–1822. https://doi.org/10.1063/1.1660449

78. Sapsford KE, Shriver-Lake LC. Bacterial Detection Using Evanescent Wave-Based Fluorescent Biosensors. In: Zourob M, Elwary S, Turner APF, editors. Principles of Bacterial Detection: Biosensors, Recognition Receptors and Microsystems. Springer-Verlag New York; 2008. p. 83–108. Available from: http://www.springer.com/br/book/9780387751122.